Dispersion of Fine Powder Agglomerates under Microgravity

A. Pyatenko, H. Takeuchi, S. Chiba, and Y. Ohyama
Hokkaido National Industrial Research Institute, Sapporo 062, Japan

Dispersion is a very important step in powder handling. Microgravity environments were applied to study the process of powder dispersion with an orifice for low transportation gas velocities and for widely sized particle agglomerates. Particle-size distributions were measured for particles after passing through the orifice, and the results were compared with the size distributions of primary particles. Data analysis showed that the main factor determining the dispersion efficiency is the inertial parameter. Two approaches are proposed for estimating the inertial parameter in a wide range of Reynolds numbers.

Introduction

When fine powders were transported by a carrying gas, large particle agglomerates rather than primary particles comprised the flow. In many cases, such a situation is not desirable, and the agglomerates need to be disrupted to produce a homogeneously dispersed system of primary particles. Such a process, known as powder dispersion, is one of the most important steps of powder preparation in many industrial processes and laboratory tests (*Powder Technology Handbook*, 1997). One of the most advanced methods is powder dispersion by orifice (Kousaka et al., 1979; Yu and Oda, 1983; Yamamoto and Suganuma, 1983). As shown by Kousaka et al. (1979), the main reason for this dispersion process is the flow acceleration. Because the drug force acting on a particle through a gas flow in Stokes's law regime is proportional to the particle's diameter d_p, but an acceleration of a particle is proportional to the particle's inverse mass m_p^{-1}, or to inverse cube of a particle diameter d_p^{-3}, the particles of different size will undergo different accelerations in a gas flow.

Pneumatic transportation of powder usually requires relatively high gas velocities (normally more than 5 m/s). The lowest transportation gas velocities were realized by Kousaka et al. (1979) and ranged from 0.35 to 3 m/s. Such low velocities were possible thanks to the special experimental scheme: a powder was not introduced directly into the system, but after a preliminary dispersion, thus, the average size of particle agglomerates transported to the orifice was kept rather small. Without such preliminary dispersion, the size of agglomerates for a fine powder could be very large, and the gas velocity for transportation of such a large particle would have to be high. High transportation gas velocities, in turn, increase the possibilities for other dispersion mechanisms, such as those by turbulence, by particle interaction with a wall, by shear stress, or by impact of particle at the orifice edge (Kousaka et al., 1979), which causes difficulties in data interpretation.

On the other hand, under microgravity environments, there are no restrictions on the size of agglomerates and/or transportation gas velocity. The only limitation for the transportation velocity is the experimental time, which in turn depends on the method of realization of microgravity conditions (that is, via a drop tower, parabolic flight, ballistic rocket or an experiment in space). Thus, by using microgravity conditions it is possible to study the dispersion mechanism for a very wide range of transportation gas velocities.

The purpose of this research is to study the process of powder dispersion by an orifice for low transportation gas velocities and for randomly sized particle agglomerates by applying microgravity conditions. A practical knowledge of the dispersion process under microgravity appears to be useful in the development of future space technologies.

Apparatus and Experimental Procedure

Three different experimental techniques for realization of microgravity conditions were applied. One group of experiments was carried out via parabolic flights, with the duration

Correspondence concerning this article should be addressed to A. Pyatenko.

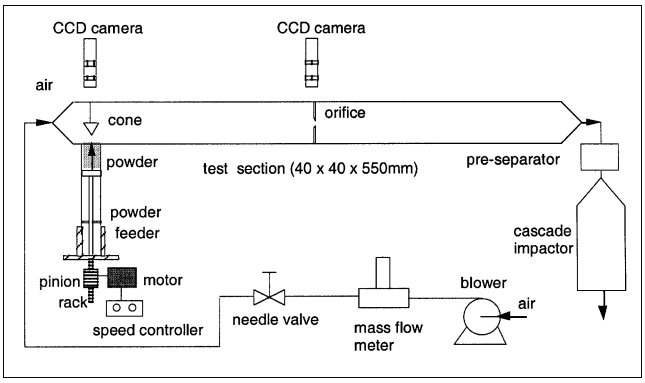

Figure 1. Experimental setup.

of each free parabolic motion of the airplane reaching 20 s, and the level of microgravity of about 10^{-2} g.

Other experiments were carried out using the drop shaft of the Japan Microgravity Center, which provides a high microgravity level of 10^{-4} g during the 10 s of the capsule's free fall, with a relatively low level of deceleration force. The capsule is of a double structure. The experimental apparatus is built in the inner capsule. There is a vacuum environment between the inner and the outer capsules, causing the inner capsule to fall freely. As it falls through air, the outer capsule is exposed to air drag. To compensate for the air drag, the outer capsule has at its end a gas thruster, which is activated during the drop.

The experiments with calcium carbonate particles (see below) were carried out using the drop facility of Micro-Gravity Laboratory of Japan, which provides a high microgravity level of about 10^{-5} g during the 4.5 s of the capsule's free fall. In the last case the capsule with the experimental apparatus falls in vacuum; therefore, the air drag is negligible during the first 4.5 s.

The experimental apparatus used in free fall experiments is shown in Figure 1. Its main components are the test section, a powder feeder, a gas line, a visualization system, and a particle-size measuring system. Such a configuration is typical for a study of the dispersion process by an orifice under normal gravity (Kousaka et al., 1979; Yuka and Oda, 1983; Yamamoto and Sugawuma, 1983). Two main principal elements, which had been designed especially for microgravity experiments, are a powder feeder and a particle-size measuring system. A piston-type feeder with a linear head motor was used for particle feeding. Before each experiment, the piston was fixed in the lowest position, and a powder in the amount of 5–7 g was placed onto it. All the apparatus then was inserted into the capsule and was ready for drop experiment. The motor was initiated by the drop command signal, which indicated the start of free fall. The piston started to move, and the supply of powder into the test section was initiated. Due to the absence of the gravitational force, and because of the low transportation gas velocities, the powder column was moved up as a solid body, while it was observed by a CCD camera. To brake down this powder column and to produce the particle agglomerates faster, the acrylic cone was used. The distance between the tip of the cone and the bottom of the test section was about 5 mm.

The orifice with a thickness of 5 mm and variable diameter of 2 to 10 mm was placed in the middle part of the test section. The particle agglomerates (or clusters) were carried out by the air flow. As the result of the very fast acceleration the clusters were subject to as the gas-solid flow passed through the orifice, the clusters were dispersed. The particle-size distributions (PSD) were measured for particles after they passed through the orifice, and the results were compared with the size distribution of primary particles.

The particle-size distribution was measured in each experiment by the cascade impactor (CI), model AS-500. The impactor was an Andersen Mark-III type (Allen, 1981) and consists of nine plates with jet nozzles of different numbers and diameters. Particles in a jet formed by such a nozzle collided with the next plate. The probability of this impact depends on the particle-size, and was calculated theoretically, as well as measured experimentally, for each plate during calibration. The geometrical characteristics of CI are shown in Table 1. The cat-size for each plate is defined by the number and diameter of nozzles at previous plate, and depends on the air-flow rate through the impactor. Preseparator was used for classification of particles larger than 30μm. Preliminary experiments were carried out to examine the ability of the cascade impactor to function in free fall experiments. Two identical CIs were exposed to the same gas-powder flow for the same duration. After that, one of them underwent free fall. Later, the particle-size distributions measured by both impactors were compared. There were no visible differences between the two distribution curves, indicating that there was no noticeable influence of microgravity and deceleration on the CI's operation.

An air flow was generated by a blower, which was switched on 10–20 s before free fall and switched off after micrograv-

Table 1. Geometrical Characteristics of Cascade Impactor

Plate No. i	No. of Nozzles N_i	Nozzle Dia. D_i, mm	Cut-size $Q = 40$ NL/min D_{p50}, μm	Cut-size $Q = 30$ NL/min D_{p50}, μm
0	264	1.6	-	-
1	264	1.2	7.60	8.80
2	264	0.92	4.96	5.70
3	264	0.72	3.24	3.75
4	264	0.54	2.21	2.57
5	264	0.35	1.39	1.61
6	264	0.25	0.70	0.81
7	156	0.25	0.42	0.49
8	264	1.0	0.27	0.32

ity conditions ceased. The air-flow rate was controlled by a needle valve and was measured by a thermal mass-flow meter. The test section was made from a transparent PMMA material for direct observation of powder feeding and transportation using two CCD cameras.

Two kinds of solid particles, white fused alumina, Al_2O_3, with average particle size of about 3 μm and calcium carbonate $CaCO_3$ with an average particle size of 0.6 μm were used in the experiments. Both powders are widely used in different powder technologies, and both are used as standard test powders in Japan (*Powder Technology Handbook*, 1997). Besides that, calcium carbonate was chosen because rather reliable data on its dispersion was obtained earlier by Kousaka et al. (1979). The characteristics of both powders are presented in Table 2.

The PSD for primary alumina particles was measured by the low angle laser light scattering method. A laser beam was projected through a stream of very dilute water-particle slurry, and the amount and direction of light scattered by the particles was measured by optical detector arrays and then analyzed by a microcomputer. A microtrac HRA model was used. Because a cascade impactor measures the particle-size distribution on a mass basis, the results of light scattering measurement were also recalculated on mass basis by using a simple assumption of particle sphericity.

When the same measurements were done for calcium carbonate powder with average particle size 0.6 mm (passport data), the results were quite different. The average size of the particle calculated from these data (1.2 μm) was about twice as large as the passport data. The differential distribution curve was not homogeneous, but looked like the superposition of few different curves. Assuming the normal distribution for the main peak, three peaks on the differential distribution curve, corresponding to monomers, dimmers, and trimmers, could be recognized. Moreover, the intensity of the dimmer peak was essentially higher than for the two others. Measurements with a different liquid (namely alcohol) gave the same results. Thus, it was possible to conclude that the fine calcium carbonate powder cannot be dispersed completely in liquids, such as water or ethanol. Therefore, the PSD of primary calcium carbonate particles is based on the data of centrifugal sedimentation analysis with photometric detection (SA-CP4L "Shimadzu" model), provided by the powder producer (Nitto Funka Trading Co.) and then recalculated on a mass basis.

Results

The results of particle-size distribution measurements for alumina particles after passing through the orifice are shown

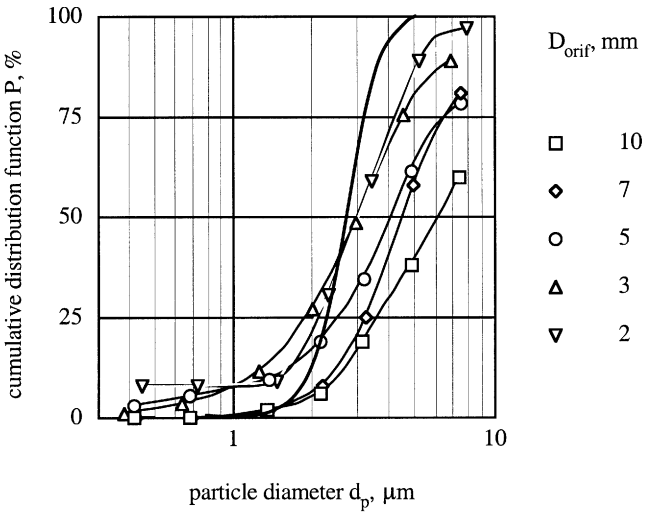

Figure 2a. Particle-size distributions measured for alumina powder after passing through the orifice.

Q_{av} = 42 NL/min. Bold line indicates the primary particle-size distribution.

in Figure 2a for average air-flow rate $Q_{av} = 42$ NL/min with different orifice diameters. For comparison, the primary particle's size distribution is shown as the bold line in the same figure. The results of similar measurements of the particle-size distribution, made for calcium carbonate powder, are shown in Figure 2b for average air-flow rate $Q_{av} = 37$ NL/min.

Comparison of Figures 2a and 2b shows that qualitatively both sets of curves have the same tendencies: the decrease in orifice diameter shifted the distribution curve to the smaller-size region. However, compared to alumina powder, the distribution curves for calcium carbonate are wider and differ more strongly from the primary particle-size distribution.

In the case of alumina powder, the prolonged tails in PSD curves were observed for small particle-sizes. This phenomenon is well known for elongated particles (Griffiths et al., 1998), since the shear flow in the region of the impactor jet tends to orientate them so that their long axes are parallel with the direction of flow and perpendicular to the impaction plate. Thus, the measured aerodynamic diameter will be greater than the correct value based on random orientation. Microscopic observation showed that the alumina particles are really elongated with an average aspect ratio of about two. This phenomenon tends to increase with decreasing of orifice diameter, because the relative amount of small parti-

Table 2. Characteristics of Powders Used in Experiments

Powder	Particle Dens. ρ_p, [kg/m^3]	Spec. Surf. Area [m$^2 \cdot$g^{-1}]	50% Median Size (in No.)* $(d_{50})_0^n$, [μm]	50% Median Size (in Mass)† $(d_{50})_0^m$, [μm]
White Fused Alumina (α-Al_2O_3)	3,950	2.7	2.10	2.71
Calcium Carbonate ($CaCO_3$)	2,700	3.5	0.60	1.15

*Results of direct PSD measurements (see text).
†Recalculated from PSDs measured in number base, by using an assumption of particle sphericity.

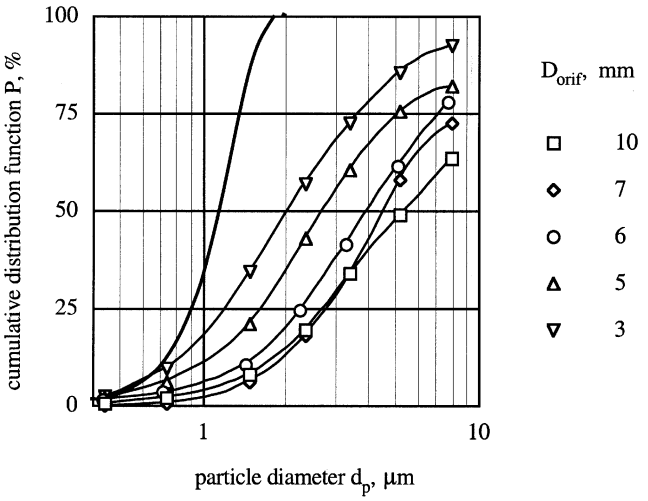

Figure 2b. Particle-size distributions measured for calcium carbonate powder after passing through the orifice.

Q_{av} = 37 NL/min. Bold line indicates the primary particle-size distribution.

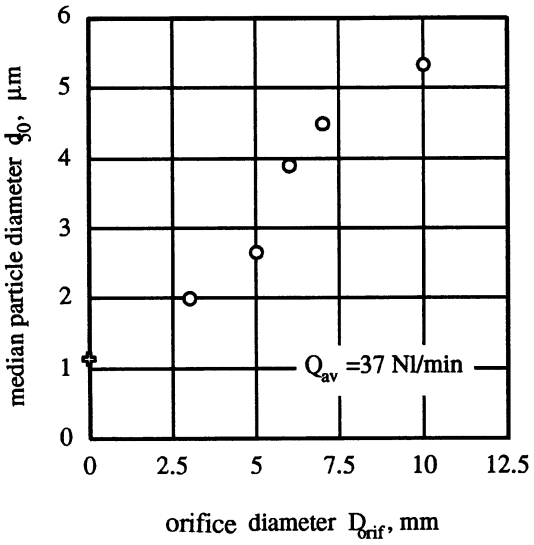

Figure 3b. Median particle diameter measured for calcium carbonate powder after passing through the orifice, vs. the orifice diameter.

cle in a flow increases when the orifice diameter decreases. Fortunately, this phenomenon does not affect the median diameter d_{50}, which can be determined as the particle size at the 50% point of each cumulative curve. The changes in median diameter vs. the orifice diameter are shown in Figures 3a and 3b for alumina and calcium carbonate powders, respectively. In both cases the median particle diameter decreases with decrease in orifice diameter, approaching the median diameter of primary particles $(d_{50})_0$. The latter values are shown as the squares on the vertical axis in the same figures.

After normalization by $(d_{50})_0$, the $(d_{50})_0/d_{50}$ ratio can be used as a measure of dispersion efficiency. The change in

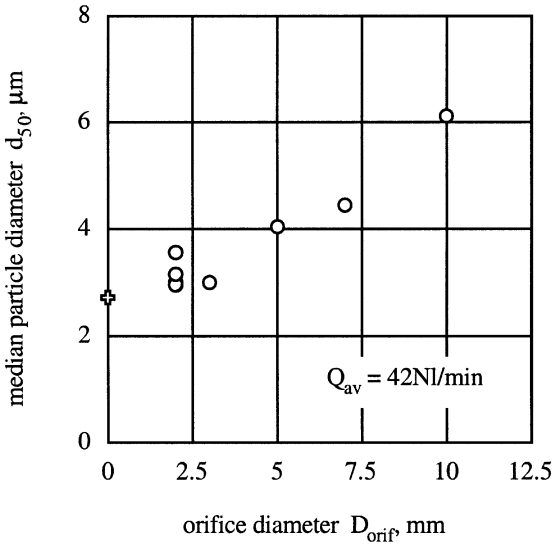

Figure 3a. Median particle diameter measured for alumina powder after passing through the orifice, vs. the orifice diameter.

dispersion efficiency defined in this way vs. the orifice diameter for alumina powder is plotted in Figure 4. As can be seen from this figure, efficiency increases with a decrease in orifice diameter and an increase in air-flow rate.

For a further discussion, it is necessary to estimate the possible errors and uncertainties of experimental data. There are three values, air-flow rate Q, orifice diameter D_{orif}, and particle median diameter d_{50}, that were measured in our experiments. The orifice diameters were measured by a microscope, and its uncertainty could be estimated as ± 0.1 mm, corresponding to $\pm 1\%$ for $D_{orif} = 10$ mm and $\pm 5\%$ for $D_{orif} = 2$ mm. The air-flow rate was measured by a thermal mass-flow meter with accuracy $\pm 1\%$. The air-flow rate was not constant, but decreased during the short time microgravity experiment, as shown in Figure 5. The reason for this flow rate decrease was high concentration of powder in the test section, which caused an additional pressure drop. Thus, the typical uncertainty in air-flow rate value was about ± 4–5% for alumina powder, and about ± 2–3% for calcium carbonate powder, because the latter was used in shorter microgravity experiments. Uncertainty in air-flow rate causes, in turn, the uncertainty in d_{50} value, because the cut-size of each plate of cascade impactor depends on the flow rate through the impactor. It is difficult to estimate all possible errors in PSD measurements or total uncertainties in d_{50} values, but one possible source is obvious: particle agglomerates could be dispersed by the nozzles of different plates of CI just the same as by orifice. To estimate the latter effect, the effective one-nozzle diameter D^* was calculated for each plate of CI as following

$$D_i^* = D_i \cdot \sqrt{N_i} \tag{1}$$

where D_i and N_i are the nozzle diameter and the number of nozzles, shown in Table 1. The possibility of using D_i^* values

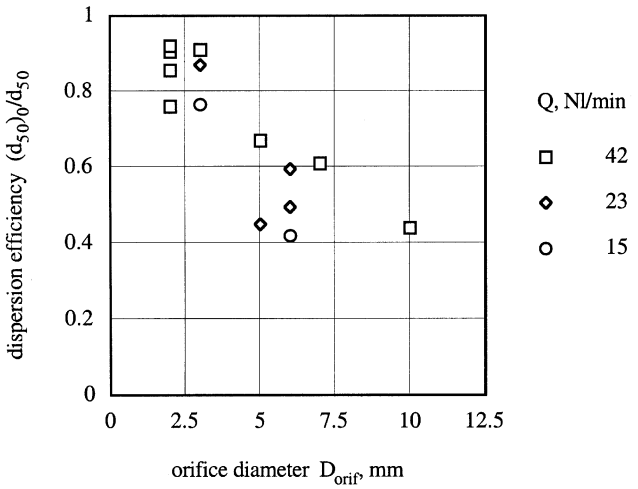

Figure 4. Dispersion efficiency vs. orifice diameter for alumina particles.

for the estimation of the dispersion efficiency in a multiorifice system was confirmed experimentally, when the multiorifices with $N = 4$, $D_{orif} = 3$ mm and with $N = 9$, $D_{orif} = 2$ mm were inserted in the test section instead of a single orifice with $D_{\text{orif}} = 6$ mm. In all three cases the effective one, orifice diameter, was constant $D^*_{\text{orif}} = 6$ mm. The dispersion efficiencies were found to be close in all three experiments. It means that a multiorifice with the same effective diameter works similar to a monoorifice in the dispersion process. Furthermore, according to Yuu and Oda (1983), in two orifices experiments of the same size, all of the agglomerates which can be disrupted under the operating conditions were disrupted at the first orifice. In our experiments with orifice diameter 2 and 3 mm no further dispersion by CI's nozzles would be

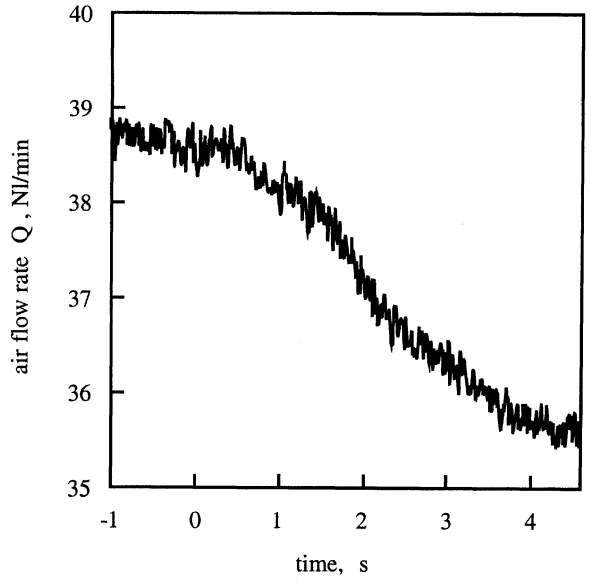

Figure 5. Decrease of the air-flow rate during the 4.5 s microgravity experiment made with calcium carbonate powder.

expected, because the minimum D_i^* value, $D_7^* = 3.1$ mm, is larger than the orifice diameters. In experiments with larger orifice diameters such additional dispersion would be possible. Thus, for example, in experiments with $D_{\text{orif}} = 7$ mm possible agglomerate dispersion could occur on the 5, 6, and 7 plates of CI. It could cause the redistribution of mass collected on the 6, 7 and 8 plates. However, because the cumulative mass on plates 6, 7 and 8 is small compared to the total mass on all plates of CI (less than 5–7%), such possible redistribution does not change the main part of the PSD curve and, hence, the d_{50} value. Finally, the uncertainties in d_{50} values caused by the uncertainties in mass, collected in different plates of CI, could be estimated as 0.1–0.2 μm, depending on the total mass on all plates of CI. Combining these values with the uncertainties caused by air-flow rate variations, the total uncertainties in d_{50} values were estimated as ± 5–7% for different experiments.

Discussion

There are few experimental works in which the dispersion efficiency was measured for different powders under different experimental conditions. Yamamoto and Suganuma (1983) presented the particle-size distribution as a function of air velocity and orifice diameter measured for four different powders. However, their data showed a systematic error, as the efficiency at many experimental points significantly exceeds one. A possible reason for this error was pointed out by the authors themselves (Yamamoto and Suganuma, 1983). They mentioned that during the sedimentation analysis of their powders, small agglomerates were sometimes observed in addition to primary particles. Yuu and Oda (1983) measured particle-size distributions before and after passing through the orifice, but did not present the data of primary particle-size distribution $(d_{50})_0$. The most reliable data were obtained by Kousaka et al. (1979), who measured the particle-size distributions for two different powders using sedimentation analysis. The authors used the same technique for measuring the particle size after passing through the orifice as well as for primary particles.

There are two experimental parameters Q and D_{orif} in any given experiment dealing with powder dispersion by an orifice. In order to compare the results reached by different authors, normally obtained under different operating conditions, it is necessary to determine a suitable universal parameter that could characterize the dispersion process. The use of the air flow energy dissipation in *vena contracta* ϵ, was proposed in Yamamoto and Suganuma (1983) for this purpose. According to Yamamoto and Suganuma (1983), the value of ϵ characterizes the intensity of the air stream through the orifice, and can be found from the following semiempirical equation

$$\epsilon\left[\text{J/m}^3\cdot\text{s}\right] = 2.7\times 10^6 Q^3/D^7_{\text{orif}}\ (Q{:}[\text{L/min}], D_{\text{orif}}{:}\ [\text{mm}]) \tag{1}$$

The physical meaning of ϵ could be explained as follows: the average kinetic energy of the unit volume of air flow in the

orifice is equal to $\rho_{air}\overline{U}^2_{orif}/2$, where

$$\overline{U}_{orif} = Q/A_{orif} = 4Q/\pi D^2_{orif} \tag{2}$$

is the mean air velocity in the orifice. By introducing the characteristic time

$$\tau_{orif} = D_{orif}/\overline{U}_{orif} \tag{3}$$

the specific energy of the air flow in the orifice per unit time will be equal to

$$\epsilon_{orif} = \frac{32\rho_{air}}{\pi^3} \cdot \frac{Q^3}{D^7_{orif}} \tag{4}$$

If the flow rate is measured in [L/min], the orifice diameter is measured in [mm], and the dimension of ϵ is measured in [J/m^3·s], the numerical coefficient in Yamamoto and Suganuma (1983) will be equal to 5.7×10^6, only twice greater than the numerical coefficient in formula (1), also defined as specific energy of the air flow, but this time at the point of maximum contraction or maximum velocity of the air flow, *vena contracta*, rather than at the orifice. In both cases the specific energy is proportional to the ratio Q^3/D^7_{orif} ratio.

Kousaka et al. (1979) used the mean air velocity in the orifice $\overline{U}_{orif}$ defined above in formula 2, as the desired characteristic parameter. Like ϵ, $\overline{U}_{orif}$ also depends only on two experimental parameters, D_{orif} and Q, but, whereas ϵ is a characteristic of the energy of the air flow in the orifice per unit time, $\overline{U}_{orif}$ is a characteristic of its momentum.

The comparison between our data and data obtained by Kousaka et al. (1979) by using the mean air velocity in the orifice as the characteristic parameter is shown in Figure 6. Four sets of data were obtained for three different powders with different average particle sizes. On number base $(d_{50})_0$ values are equal to 0.64 μm and 0.31 μm for calcium carbonate and iron oxide respectively, and, after recalculation on mass base, they are equal to 0.9 μm and 0.36 μm, respectively. Our data for calcium carbonate powder is very close to the data presented by Kousaka et al. (1979), obtained for the same powder, but by using a different method for measuring the particle size distribution. One can see that our dispersion data for alumina powder was obtained for a wider range of mean air velocities. It has become possible to enlarge the range of $\overline{U}_{orif}$ values essentially by applying microgravity conditions.

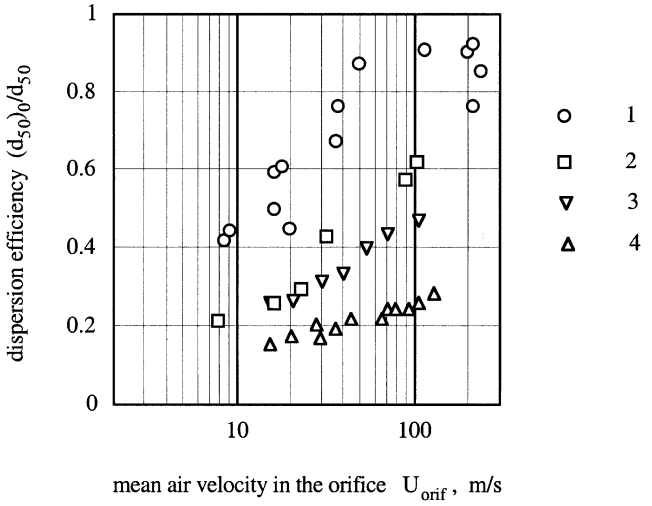

Figure 6. Dispersion efficiency vs. mean air velocity in the orifice.

1: Our data, Al_2O_3, 2: our data, $CaCO_3$, 3: Kousaka et al. (1979), $CaCO_3$, 4: Kousaka et al. (1979), Fe_2O_3.

The dispersion efficiency increases as the average size of the particles increases. Thus, it is possible to conclude that the dispersion efficiency depends not only on the operating conditions, but on the powder properties as well. And, to approximate the dispersion data for different powders by one universal equation, it is necessary to use a universal parameter that depends not only on D_{orif} and Q values, but on powder properties, such as particle diameter and, perhaps, density as well. Moreover, this universal parameter seems to be dimensionless.

There are two dimensionless parameters: inertial parameter φ and particle Reynolds number Re_p; both depend on particle diameter, d_p. The inertial parameter is defined as the ratio of the particle velocity response time τ_0 to the process characteristic time, defined above by Eq. 3. In Stokes flow regime the particle velocity response time is equal to $\tau_0 = \rho_p d^2_p/18\mu$ and, then, the value of inertial parameter will be equal to

$$\varphi = \frac{\rho_p d^2_p \overline{U}_{orif}}{18\mu D_{orif}} \tag{5}$$

If $\varphi \ll 1$, the particles will have ample time to respond to changes in flow velocity, and, thus, the particles and fluid velocity changes will be nearly equal. On the other hand, if this parameter far exceeds 1, the particle will have essentially no time to respond to the fluid velocity changes and the particle velocity will be little affected during its passage through the orifice.

Particle Reynolds number

$$\mathrm{Re}_p = \frac{\rho_g d_p (U_g - U_p)_{orif}}{\mu} \tag{6}$$

is the characteristic of the relative fluid-particle moving conditions. When $\mathrm{Re}_p < 1$, the viscous force is dominated in the fluid-particle interaction. This flow is regarded as a creeping flow, and this region of particle Reynolds numbers is known as Stokes flow regime. For $\mathrm{Re}_p > 500$, the inertia term is dominated in fluid-particle interaction and the flow regime is known as Newton's. Because the Re_p value is proportional to a particle slip velocity $U_g - U_p$, it strongly depends on the value of inertial parameter.

On the other hand, the expression and the value of inertial parameter φ strongly depends on the flow regime and, therefore, on the Re_p value. Usually, the expression (Eq. 5), valid only for Stokes flow regime, is shown in literature. If the range of Re_p values slightly exceeds 2, it is possible to use the fol-

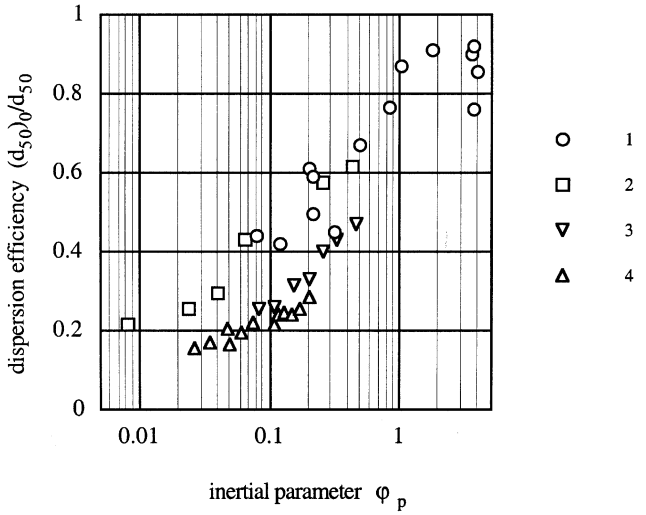

Figure 7. Dispersion effciency vs. inertial parameter for primary particle, calculated by cyclic using formulas 5-8.

Symbols 1–4 have the same meaning as in Figure 6.

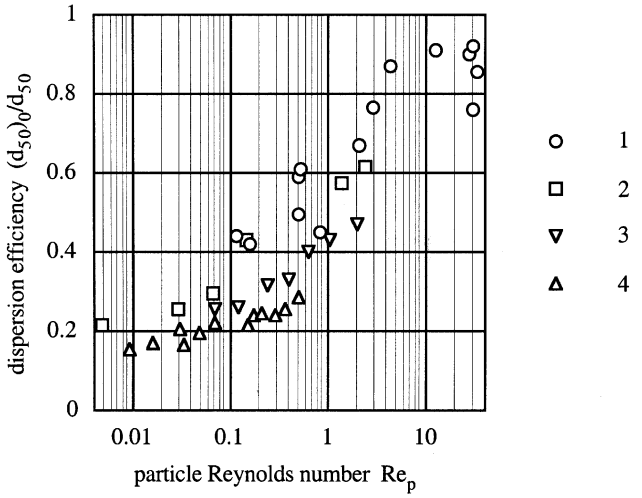

Figure 8. Dispersion efficiency vs. particle Reynolds number, calculated by cyclic using formulas 5-8.

Symbols 1–4 have the same meaning as in Figure 6.

lowing approach: First, the values of inertial parameter $\varphi^{(0)}$ are calculated in the assumption of Stokes regime using the formula (Eq. 5). Then, the particle slip velocities could be estimated by using the formula

$$U_g - U_p = U_g \cdot \frac{\varphi}{1+\varphi} \tag{7}$$

whose validity for Stokes regime is shown, for example, in Growe et al. (1998). Next, the R_p values could be calculated by using the formula (Eq. 6). Finally, the correction in inertial parameter values could be made by using the Schiller-Naumann formula

$$\varphi^{(1)} = \varphi^{(0)} / \left(1 + 0.15 \cdot Re_p^{0.687}\right) \tag{8}$$

This procedure then could be repeated until the asymptotic φ and Re_P values are reached. In fact, three–four cycles are enough to get an accuracy of approximately a few percent. The dispersion efficiency plotted against the inertial parameter, calculated by using this approach, is shown in Figure 7. In spite of the large data scattering, it is possible to see that two sets of our data obtained for alumina and calcium carbonate are very close to each other, and differ from two sets of data obtained by Kousaka et al. (1979) for calcium carbonate and iron oxide, which, in turn, also are close to each other. All four sets of data have near the same slope in logarithmic scale used in this figure. The shift between the data observed in Figure 7, obtained under normal gravity and under microgravity conditions, corresponds to factor 4 in inertial parameter. The same tendency will be observed if the dispersion efficiency is plotted against the particle Reynolds number, but the different slopes could be recognized for each set of data, as shown in Figure 8. As it can be seen from Figure 8, all of Kousaka et al. (1979) data, as well as our data for calcium carbonate, correspond to the Stokes regime, and the corrections had to be made mainly for alumina powder data.

To explain these results, we estimate, following Yu and Oda (1983), that the dispersion process of particle agglomerate due to acceleration through an orifice occurs for a much shorter time than that of particle acceleration through an orifice. In such a case, the particle agglomerate moves in a gas flow until dispersion takes place, and, therefore, the relative agglomerate, which is air movement, and not primary particle movement, must be the main factor responsible for the dispersion process. Therefore, the average size and density of the agglomerate and not the primary particle must be used in Eq. 5. In such a case, the results shown in Figure 7 could be interpreted as follows:

(1) The average size and density of agglomerates are proportional to the size and density of primary particles. The density of the agglomerate was assumed to be equal to that of the primary particle. It means that the average agglomerate diameter is the volume equivalent diameter (Allen, 1981).

(2) For the same experimental environment (that is, our microgravity experiments or experiments by Kousaka et al. (1979)) the proportionality factor is the same for different powders.

(3) For the same powder (that is, calcium carbonate) in our microgravity experiments, the size proportionality factor is about twice as large as in experiments by Kousaka et. al. (1979). It is in qualitative agreement with the different powder feeding systems used in these two experimental schemes (see above).

The average agglomerate diameter could not be measured in our experiments, because of the restrictions for CI measurements (see Table 1). In experiments made without any orifice most of the particles were collected on the plates number 0 and 1, as it was impossible to measure the PSD. The lowest limit for average agglomerate diameter can be estimated for iron oxide power as 2.5 μm, because the dispersion efficiency for this powder was already very low and

the maximum d_{50} value was measured as 2.0 μm. Assuming the same proportionality factor κ in the equation

$$d_{ag} = \kappa d_p \tag{9}$$

for all experiments made by Kousaka et al. (1979), and assuming twice the larger factor for all our experiments, the lowest limits for three other sets of experiments could be found as follows: 6.2 μm for calcium carbonate studied by Kousaka et al. (1979), 16.0 μm for calcium carbonate studied in our experiments, and 37.6 μm for alumina powder. For such large sizes of agglomerate particles, the values of inertial parameter and particle Reynolds number could be very large, and a different approach to estimation of these parameters could be proposed.

The expression for inertial parameter in Stokes flow regime (Eq. 5) could be easily obtained from the solution of the particle motion equation in this regime by assuming that the gas velocity sharply increases from 0 to a constant value U_g

$$U_p = U_g(1 - e^{-t/\tau_0}) \tag{10}$$

In the same assumption $U_g = \text{const}$ the solution of particle motion equation in Newton's regime will be

$$U_p = U_g \cdot \frac{t/\tau_0}{1 + t1/\tau_0} \tag{11}$$

where

$$\tau_0 = 3 \cdot \frac{\rho_p d_p}{\rho_g U_g} \tag{12}$$

Therefore, in Newton's flow regime, the expression for inertial parameter will be equal to

$$\varphi = 3 \cdot \frac{\rho_p d_p}{\rho_g D_{\text{orif}}} \tag{13}$$

The following expression for inertial parameter valid for both regimes, could then be proposed as

$$\varphi = \frac{\rho_p d_p}{\rho_g D_{\text{orif}}} \cdot \frac{3 \cdot Re_p^*}{Re_p^* + 3 \cdot 18} \tag{14}$$

where

$$Re_p^* = \frac{\rho_g d_p U_{\text{orif}}}{\mu} = Re_p \frac{U_{\text{orif}}}{(U_g - U_p)_{\text{orif}}} = Re_p \cdot \frac{\varphi + 1}{\varphi} \tag{15}$$

When $Re_p^* \gg 54$, the inertial parameter will be expressed by formula 13. When $Re_p^* \ll 54$, formula 5 will be valid. Because large Re_p^* values correspond to the large values of the inertial parameter, and, thus, for large Re_p^* values, $Re_p^* \cong Re_p$, the $Re_p^* \gg 54$ condition corresponds to $Re_p \gg 54$, and then approximately to $Re_p > 500$ (Newton's flow regime). For small Re_p^* values, $\varphi \leq 1$, and according to formula 15, the Re_p values became twice as small as Re_p^*. Therefore, the $Re_p^* \ll 54$ condition corresponds to $Re_p^* < 5$, and then approximately to $Re_p < 2$ (Stokes flow regime).

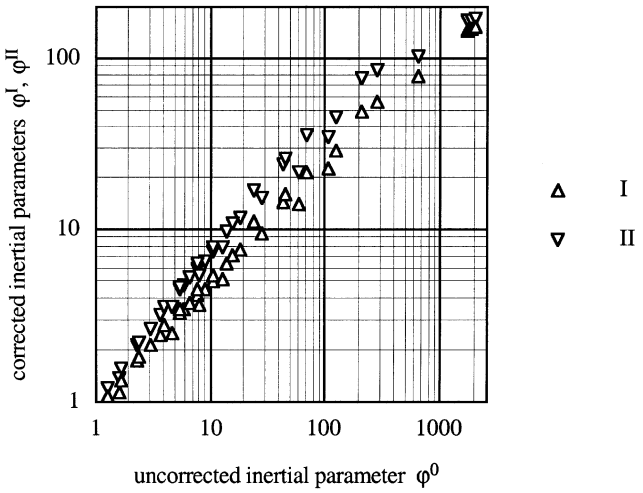

Figure 9. Values of inertial parameter, calculated by using formulas 8 and 14, against the uncorrected values, calculated by using the formula 5.

The comparison between values of inertial parameter calculated by using different approaches is shown in Figure 9, where φ^{I} and φ^{II} values, calculated by using the Schiller-Naumann correction 8, and by using the formula 14, respectively, are plotted against the uncorrected φ^0 values, calculated by using Formula 5. Both approaches give rather close results. For large values of inertial parameter, both approaches give essentially smaller results compared to the uncorrected values. Thus, for large values of inertial parameter, or for large values of the particle Reynolds number, the correction is absolutely necessary, and either approach to such a correction could be used.

The dispersion efficiency as a function of inertial parameter of particle agglomerate φ_{ag} is shown in Figure 10. The lowest limits of average agglomerate diameter estimated above are used as d_p values in Eqs. 14 and 15. Thus, the φ_{ag} values are defined with unknown coefficient $k > 1$, which corresponds to a possible right shift of all the data in logarithmic scale used in Figure 10. In spite of the large scattering of the data, especially data for alumina powder obtained for large values of inertial parameter, it is possible to approximate all the data by one S-shape curve. For large dispersion efficiency, the absolute values of inertial parameter of particle agglomerate φ_{ag} have to be rather large. To have the efficiency of about 0.5, it is needed to provide φ_{ag}values larger than 30.

For a more quantitative understanding of the dispersion process, the knowledge of the average sizes of particle agglomerates is necessary. Therefore, more experiments with different powders have to be done in a wide range of the inertial parameter with measurements of the particle-size distributions made before and after passing through an orifice. Of course, these experiments could be performed under nor-

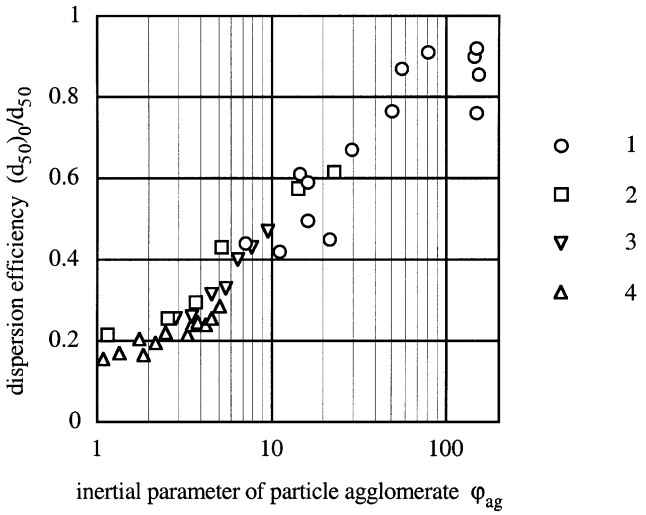

Figure 10. Dispersion efficiency vs. inertial parameter of particle agglomerate.

Symbols 1–4 have the same meaning as in Figure 6.

mal gravity conditions, but the particle feeding systems in these experiments have to produce the agglomerate with large average size.

Finally, the advantage of using the microgravity conditions could be explained as the following: The dispersion efficiency is proportional to the $U_{\text{orif}}/D_{\text{orif}}$ ratio, or, because $U_{\text{orif}} \propto Q/D^2_{\text{orif}}$, to the Q/d^3_{orif} ratio. On the other hand, the pressure drop on the orifice is proportional to the Q^2/D^4_{orif} ratio (see, for example Yamamoto and Suganuma (1983). Then, to increase the dispersion efficiency for the same pressure drop, it is necessary to decrease the orifice diameter and simultaneously to decrease the gas flow rate as a square root of the orifice diameter. However, the decrease in gas-flow rate or in transportation gas velocity has a limitation under gravity condition as was mentioned above. Under microgravity, it is possible to obtain high dispersion efficiencies by operating with small diameter orifices, and by keeping a suitable pressure drop on the orifice by operating with low flow rates.

Conclusions

The following conclusions could be made:

(1) The dispersion efficiency depends on the inertial parameter of particle agglomerates. To calculate the φ_{ag} values, the average size of agglomerates has to be known. After that, φ_{ag} could be calculated by using the formulas 14, 15, or by cyclic using the formulas 5–8. For a particular experimental scheme, the inertial parameter of primary particles, φ_p can be used as a measure of dispersion efficiency, because the same φ_p values correspond to the same dispersion efficiency for the different powders.

(2) For different experimental schemes, larger dispersion efficiency could be expected for experiments where the feeding system produces the largest sizes of particle agglomerates.

(3) Because the average size of agglomerates seems to be proportional to the average size of the primary particles, for experiments with the same material, larger efficiency could be expected for larger size primary particles. The fine powder is more difficult to disperse compared to the coarse powder of the same material.

(4) For a particular powder (d_p and ρ_p values are fixed), the dispersion efficiency depends on the $U_{\text{orif}}/D_{\text{orif}}$ ratio, or, because $U_{\text{orif}} \propto Q/D^2_{\text{orif}}$, on the Q/D^3_{orif}. Therefore, the most critical experimental parameter is the orifice diameter. Moreover, because the experimental conditions in which the efficiency is close to one are closer to Newton's flow regime where $\varphi \rightarrow \rho_p d_p/\rho_g D_{\text{orif}}$, increasing the gas-flow rate becomes ineffective, and the only possible way to approach very high dispersion efficiency is to decrease the orifice diameter.

Literature Cited

Powder Technology Handbook, 2nd ed., K. Gotoh, H. Masuda and K. Higashitani, eds., Marcel Dekker, New York (1997).

Kousaka, Y., K. Okuyama, A. Shimizu, and T. Yoshida, "Dispersion Mechanism of Aggregate Particles in Air," *J. Chem. Eng. Japan*, 12, 152 (1979).

Yuu, S., and T. Oda, "Disruption Mechanism of Aggregate Aerosol Particles through an Orifice," *AIChE J.*, **29**, 191 (1983).

Yamamoto, H., and A. Suganuma, "Dispersion of Aggregated Airborne Dust by Orifice," *Kagaku Kogaku Ronbushu*, **9**, 183 (1983).

Allen, T., "Particle-Size Measurement," 3rd ed., Chapman and Hall, London (1981).

Griffiths, W., D. Mark, I. Marshall, and A. Nichols, *Aerosol Particle Size Analysis*, The Royal Society of Chemistry, London (1998).

Growe, C., M. Sommerfeld, and Y. Tsuji, "Multiphase Flows with Droplets and Particles," CRC Press, Boca Raton, FL (1998).

Manuscript received Sept. 28, 2000, and revision received June 4, 2001.